Ozone Pollution over China and India: Seasonality and Sources

Meng Gao[1,2,3], Jinhui Gao[4], Bin Zhu[3], Rajesh Kumar[5], Xiao Lu[2], Shaojie Song[2], Yuzhong Zhang[2], Beixi Jia[1], Peng Wang[6], Gufran Beig[7], Jianlin Hu[8], Qi Ying[6], Hongliang Zhang[9], Peter Sherman[10], and Michael B McElroy[2,10]

1 Department of Geography, State Key Laboratory of Environmental and Biological Analysis, Hong Kong Baptist University, Hong Kong SAR, China
2 John A. Paulson School of Engineering and Applied Sciences, Harvard University, Cambridge, MA, United States
3 Key Laboratory for Aerosol-Cloud-Precipitation of China Meteorological Administration, Nanjing University of Information Science and Technology, Nanjing, China
4 Department of Ocean Science and Engineering, Southern University of Science and Technology, Shenzhen, China
5 National Center for Atmospheric Research, Boulder, CO, USA
6 Zachry Department of Civil Engineering, Texas A&M University, College Station, TX 77843-3136, USA
7 Indian Institute of Tropical Meteorology, Pune, India
8 School of Environmental Science and Engineering, Nanjing University of Information Science & Technology, 219 Ningliu Road, Nanjing 210044, China
9 Department of Environmental Science and Engineering, Fudan University, Shanghai 200438, China
10 Department of Earth and Planetary Sciences, Harvard University, Cambridge, MA, United States

Correspondence: Meng Gao (mmgao2@hkbu.edu.hk) and Michael B. McElroy (mbm@seas.harvard.edu)

Abstract

A regional fully coupled meteorology-chemistry Weather Research and Forecasting model with Chemistry (WRF-Chem) was employed to study the seasonality of ozone (O_3) pollution and its sources in both China and India. Observations and model results suggest that O_3 in the North China Plain (NCP), Yangtze River Delta (YRD), Pearl River Delta (PRD) and India exhibit distinctive seasonal features, which are linked to the influence of summer monsoons. Through a factor separation approach, we examined the sensitivity of O_3 to individual anthropogenic, biogenic, and biomass burning emissions. We found that summer O_3 formation in China is more sensitive to industrial and biogenic sources than to other source sectors, while the transportation and biogenic sources are more important in all seasons for India. Tagged simulations suggest that local sources play an important role in the formation of the summer O_3 peak in the NCP, but sources from Northwest China should not be neglected to control summer O_3 in the NCP. For the YRD region, prevailing winds and cleaner air from the ocean in summer lead to reduced transport from polluted regions, and the major source region in addition to local sources is Southeast China. For the PRD region, the upwind region is replaced by contributions from polluted PRD as autumn approaches, leading to an autumn peak. The major upwind regions in autumn for the PRD are YRD (11%) and Southeast China (10%). For India, sources in North India are more important than sources in the south. These analyses emphasize the relative importance of source sectors and regions as they change with seasons, providing important implications for O_3 control strategies.

1 Introduction

Tropospheric ozone (O_3) is the third most potent greenhouse gas in the atmosphere (*Pachauri and Reisinger, 2007*), an important surface air pollutant, and the major source of the hydroxyl radical (a key oxidant playing an essential role in atmospheric chemistry). With the rapid growth of industrialization, urbanization and transportation activities, emissions of O_3 precursors (nitrogen oxides and volatile organic compounds) in both China and India have increased significantly since 2000 (*De Smedt et al., 2010; Duncan et al., 2014; Hilboll et al., 2013; Kurokawa et al., 2013; Ohara et al., 2007; Stavrakou et al., 2009; Zheng et al., 2018*).

Increasing concentrations of O_3 precursors have led to emerging and widespread O_3 pollution, threatening health and food security (*Chameides et al., 1994; Malley et al., 2018*). The decrease in crop yield resulting from the increase in surface O_3 would have been sufficient to feed 95 million people in India (*Ghude et al., 2014*).

Great efforts have been devoted to improving understanding of exceptionally high concentrations (*Wang et al., 2006*) and the increasing trend in O_3 for both China and India (*Beig et al., 2007; Cheng et al., 2016; Ghude et al., 2008; Lu et al., 2018a; Ma et al., 2016; Saraf and Beig, 2004; Xu et al., 2008*). Strong but distinctive seasonal variations of O_3 observed in India and China have been linked to higher emissions of precursor gases (*Lal et al., 2000*), and summer monsoon (*Kumar et al., 2010; Lu et al., 2018b; Wang et al., 2017*). The contributions of individual economic sectors and source regions were reported based on sensitivity simulations and source apportionment techniques (*Gao et al., 2016a; Li et al., 2008; Li et al., 2016; Li et al., 2012; Lu et al., 2019; Wang et al., 2019*). With respect to the enhanced concentrations of O_3 over the past years, *Sun et al. (2019)* attributed this to elevated emissions of anthropogenic VOCs, while *Li et al. (2019)* argued that an inhibited aerosol sink for hydroperoxyl radicals induced by decreased $PM_{2.5}$ over 2013-2017 played a more important role in the NCP.

Despite these progresses, the seasonal behaviors of O_3 in different regions greatly differ, yet have not been intercompared and the underlying causes have not been comprehensively explored. In addition, previous source apportionment studies focused on specific regions or episodes, and the policy implications drawn from these studies might not be applicable for other regions and seasons. It is both of interest and of significance to understand the similarities and differences between O_3 pollution in China and India, the two most polluted and most populous countries in the world.

The present study uses a fully online coupled meteorology-chemistry model (WRF-Chem) to examine the general seasonal features of O_3 pollution, and its sources derived from economic sectors and regions over both China and India. Sect. 2 describes the air quality model and measurements. We examine then in Sect. 3 how the model captures the spatial and temporal variations of O_3 and relevant precursors. Sect. 4 presents general seasonal features of O_3 pollution, and the relative importance of both economic sectors and source regions. Results are

discussed and summarized in Sect. 5.

2 Model and data

2.1 WRF-Chem model and configurations

The fully online coupled meteorology-chemistry model WRF-Chem (*Grell et al., 2005*) was employed in this study using the CBMZ (Carbon Bond Mechanism version Z, *Zaveri and Peters, 1999*) photochemical mechanism and the MOSAIC (Model for simulating aerosol interactions and chemistry, *Zaveri et al., 2008*) aerosol chemistry module. The model was configured with a horizontal grid spacing of 60km with 27 vertical layers (from the surface to 10 hPa), covering East and South Asia (Fig. 1). The selected physical parameterization schemes follow the settings documented in *Gao et al. (2016b)*, and they are listed in Table S1. Meteorological initial and boundary conditions were obtained from the 6-hourly FNL (final analyses, *NCEP, 2000*) global analysis data with 1.0°×1.0° resolution. The four-dimensional data assimilation (FDDA) technique was applied to limit errors in simulated meteorology. Horizontal winds, temperature and moisture were nudged at all vertical levels. Chemical initial and boundary conditions were provided using MOZART-4 (*Emmons et al., 2010*) global simulations of chemical species.

Monthly anthropogenic emissions of SO_2, NO_x, CO, NMVOCs (Non-methane Volatile Organic Compounds), NH_3, $PM_{2.5}$, PM_{10}, BC (black carbon) and OC (organic carbon) were taken from the MIX 2010 inventory (*Li et al., 2017*), a mosaic Asian anthropogenic emission inventory covering both China and India. In this study, the emissions in China were updated with the MEIC (Multi-resolution Emission Inventory for China, http://www.meicmodel.org/) inventory for year 2012. From 2012 to 2013, emissions of SO_2 and NO_x in China declined by 11% and 5%, while emissions of other species did not exhibit a significant change (*Zheng et al., 2018*). The MIX inventory was prepared considering five economic sectors on a 0.25°×0.25° grid: power, industrial, residential (heating, combustion, solvent use, and waste disposal), transportation and agriculture. For India, SO_2, BC, OC, and power plant NO_x emissions were taken from the inventory developed by the Argonne National Laboratory (ANL), with the REAS (Regional Emission inventory in Asia) inventory used to supplement for missing species. Speciation mapping of VOCs emissions follows the speciation framework documented in *Li et*

al. (2014) and *Gao et al. (2018)*. The MEGAN (Model for Emissions of Gases and Aerosols from Nature, *Guenther et al., 2012*) model version 2.04 was used to generate biogenic emissions online. Biomass burning emissions were obtained from the 4th generation global fire emissions database (GFED4, *Giglio et al., 2013*). For China, industrial and power sectors are the largest two contributors to NO_x emissions, while industrial sector emits the largest amounts of NMVOCs (*Li et al., 2017*). For India, transportation and power sectors produce the largest amounts of NO_x, while residential and transportation sectors are the largest two contributors to NMVOCs emissions (*Li et al., 2017*). China's biogenic emissions of VOCs are estimated to be comparable to or higher than anthropogenic sources (*Li and Xie, 2014; Wei et al., 2011*).

2.2 Ozone tagging method and setting of source regions

O_3 observed in a particular region is a mixture of O_3 formed by reactions of NO_x with VOCs emitted at different locations and time. The O_3 tagging method has the capability to apportion contributions of different source regions to O_3 concentrations observed in particular regions. The present study adopted the ozone tagging method implemented in WRF-Chem by *Gao et al. (2017a)*, which is similar to the Ozone Source Apportionment Technology (OSAT, *Yarwood et al., 1996*) approach implemented in the Comprehensive Air Quality Model with extensions (CAMx). Both O_3 and its precursors from different source regions are tracked as independent variables. The ratio of formaldehyde to reactive nitrogen oxides ($HCHO/NO_y$) was used as proposed by *Sillman (1995)* to decide whether the grid cell is under NO_x or VOC limited conditions, and then different equations for these two conditions were selected to calculate total O_3 chemical production. A detailed description of the technique is provided in *Gao et al. (2017a)*.

The O_3 tagging method attributes production of O_3 and its precursors to individual geographic areas. We divided the entire modeling domain into 23 source regions, which were classified mainly using the administrative boundaries of provinces. In eastern China, each province was considered as a source region, while provinces in northeastern, northwestern, and southwestern China were lumped together (Fig. S1). India was divided into two source regions (north and south), and other countries were considered separately as a whole (Fig. S1). Additionally, the chemical boundaries provided by MOZART-4 were adopted to specify inputs of O_3, and the

initial condition was tracked also as an independent source. The names of all source groupings are indicated in Fig. S1.

2.3 Experiment design

To quantify the sectoral contributions to O_3, a factor separation approach (FSA) was applied to differentiate two model simulations: one with all emission sources considered, and the other with some emission sources excluded. Table 1 summarizes the different sets of simulations conducted in this study. In addition to the control case, a series of sensitivity studies was performed, in which industrial, residential, transport, power, biogenic and fire emissions were separately excluded (Table 1). For each case, the entire year of 2013 was simulated.

2.4 Measurements

Surface air pollutants in China are measured and recorded by the Ministry of Environmental Protection (MEP), and the data are accessible on the China National Environmental Monitoring Center (CNEMC) website (http://106.37.208.233:20035/). This nationwide network was initiated in January 2013, and this dataset was used to evaluate model performance. This dataset has been extensively employed in previous studies to understand the spatial and temporal variations of air pollution in China (*Hu et al., 2016; Lu et al., 2018a*), and to reduce uncertainties in estimates of health and climate effects (*Gao et al., 2017b*). Measurements of air pollutants from the MAPAN network (Modeling of Atmospheric Pollution and Networking) set up by the Indian Institute of Tropical Meteorology (IITM) under project SAFAR (System of Air Quality and weather Forecasting And Research) (*Beig et al., 2015*) were used in the present study to evaluate the model performance over India. To further evaluate how the model performed in capturing the vertical distributions of O_3, we used data from ozonesonde records obtained from the World Ozone and Ultraviolet Radiation Data Center website (https://woudc.org/data/dataset_info.php?id=ozonesonde). Fig. 1 displays the locations of the relevant surface and ozonesonde observation sites. We evaluated also the spatial distribution of NO_2 columns using the KNMI-DOMINO (Dutch OMI NO_2) daily level-2 products of tropospheric NO_2 column (www.temis.nl), with row anomaly removed (according to operational flagging), solar zenith angles less than 80º, and cloud fraction less than 0.2. The

model results were sampled according to selected satellite data on a pair-to-pair basis. The matched model results were transformed by applying the OMI averaging kernel to the modeled vertical profiles of NO_2 concentrations.

3 Model evaluation

We evaluated the spatial distribution of simulated seasonal mean (winter months include January, February and December (DJF); spring months include March, April and May (MAM); summer months include June, July and August (JJA); Autumn months include September, October, and November (SON)) O_3 concentrations by comparing model results with observations (filled circles in Fig. 2) for 62 cities in China and India. The model captures the spatiotemporal patterns of O_3 in east China, with lower values in fall (Fig. 2d) and winter (Fig. 2a), and enhanced levels in spring (Fig. 2b) and summer (Fig. 2c). However, O_3 concentrations are overestimated by the model in central, northwest and southwest China for all seasons (Fig. 2). *Hu et al. (2016)* reported also that their model tends to predict higher O_3 concentrations for these regions. Scatter plots of simulated and observed O_3 for four seasons suggest that model overestimates O_3 in most sites during winter, and exhibit better performance during other seasons (Fig. 3). Fig. S2 indicates that modeled NO_2 column values in east China are not as high as observed, but model overpredicts NO_2 column in central China and most parts of India, which could partly explain the overestimation of O_3 in central China.

We conducted a further site-by-site evaluation of monthly mean O_3 concentrations, and we grouped stations into four major densely-populated regions, namely North China Plain (NCP), Yangtze River Delta (YRD), Pearl River Delta (PRD), and India. The seasonality of observed O_3 concentrations is reproduced well in these four regions (Fig. 4), although concentrations are underestimated in the NCP in spring. O_3 concentrations in October, November and December in the PRD region are overestimated by the model. The correlation coefficients between model and observations range between 0.84 and 0.98. Detailed model evaluation statistics are documented in Table 2. In Beijing, the daily maximum 8-h average (MDA8) O_3 concentrations are well captured by the model (Fig. S3), except that the model is biased low in spring. Stronger NO_x titration (underestimation of O_3 during the night, Fig. S4) are found in the model results for the NCP and YRD regions in spring, which can partly explain the underestimation of O_3 in

spring in the NCP and PRD (Fig. S4). The simulated magnitudes of O_3 in India are generally consistent with observations, though lower in central India and in May. The high concentrations of O_3 in India were not captured by the model is mainly because of the large underestimation in Jabalpur (Central India) with complex terrain. Model's coarse resolution and poor capability of resolving strong spatial heterogeneity in land types within a small area have led to this mismatch, which was also found in *Sharma et al. (2017)*. Fig. 4 suggests also that the seasonal behavior of O_3 in these four major regions exhibits distinctive patterns, discussed in detail in Sect. 4.

In this work, ozonesonde measurements from the Hong Kong Observatory (HKO), Japan Meteorological Agency (JMA), and the Hydrometeorological Service of S.R. Vietnam (HSSRV) (locations marked in purple in Fig. 1) were used. Wintertime near-surface O_3 concentrations are overestimated for HKO (Fig. S5), while vertical variations are satisfactorily captured by the model. Comparisons of near-surface O_3 precursors suggest that CO concentrations are underestimated in all the regions (Fig. S6), which could be explained by an underestimate of CO emissions (*Wang et al., 2011*). The coarse grid resolution of the model might provide another reason for this underestimation, as the observation sites in China are located mostly in urban areas. Underestimates of CO concentrations are reported also for many sites in India (*Hakim et al., 2019*). The effects of underestimated CO on O_3 were found to be small, but the underestimation of CO may lead to bias in methane lifetime (*Strode et al., 2015*), which is beyond the discussion of regional pollution in this study. Simulated NO_2 concentrations are slightly overestimated in the NCP but are underestimated in the PRD (Fig. S6). Despite these issues, the model still captures the seasonal behavior of O_3 in different regions, and we do not expect the model biases to change the major findings of the present study.

4 Seasonality, source sectors and source regions

4.1 Seasonality of surface O_3 in different regions

Comparisons between modeled and observed near-surface O_3 concentrations for different regions suggest distinctive seasonal patterns (Fig. 4). Over the NCP, near-surface O_3 exhibits an inverted V-shaped pattern, with maximum O_3 concentrations in summer, minimum in winter (Fig. 4). Over the YRD, O_3 presents a bridge shape, with relatively higher concentrations in

spring, summer and autumn (Fig. 4). O_3 concentrations over the PRD peak in autumn, with a minimum in summer (Fig. 4). Similarly, O_3 over India exhibits a minimum in summer, with highest concentrations in winter (Fig. 4).

China and India are influenced largely by monsoonal climates (*Wang et al., 2001*), and the seasonality of O_3 in different regions is affected by wind pattern reversals related to the winter and summer monsoon systems (*Lu et al., 2018b*). Various monsoon indices have been proposed to describe the major features of the Asian monsoon, based on pressure, temperature, and wind fields, etc. In the present study, we adopted the dynamical normalized seasonality monsoon index (DNSMI) developed by *Li and Zeng (2002)* to explore the influence of monsoon intensity on the seasonal behavior of O_3 in the boundary layer in different regions of China and India. DNSMI is defined as follows:

$$DNSMI = \frac{\|\overline{V_1} - V_i\|}{\bar{V}} - 2 \quad (1)$$

in which V_1 and V_i represent the wind vectors in January, and wind vectors in month i, respectively. $\bar{V}$ denotes the mean of wind vectors in January and July. The norm of a given variable is defined as:

$$\|A\| = (\int\int |A|^2 dS)^{\frac{1}{2}} \quad (2)$$

where S represents the spatial area of each model grid cell. More detailed information on the definition is presented in *Li and Zeng (2002)*.

This definition of monsoon proposed by *Li and Zeng (2002)* focuses on wind vectors, representing the intensity of wind direction alternation from winter to summer. In winter, northwesterly winds are predominant, then higher DNSMI values indicate stronger alternation of wind directions. For example, DNSMI values are higher than 5 in coastal regions of South China and most environments in India (Fig. 5c), suggesting that these regions are influenced largely by the summer monsoon. The spatial distribution of monsoon precipitation in Fig. S7(c) also indicates that most areas of India and South China are influenced by summer monsoon. The alternation of wind vectors (Fig. 5) and precipitation (Fig. S7) from winter to summer results in changes in upwind areas and abundance of O_3 precursors, modulating the severity of O_3 pollution. In summer, the southerly winds containing clean maritime air masses, serve to reduce the intensity of pollution in regions that are affected largely by the summer monsoon

(e.g., most regions over India, and coastal regions of China). Besides, summer monsoon can bring about cloudy and rainy weather conditions (Fig. S7, removement of ozone precursors), weaker solar radiation, and lower temperature (Lu et al., 2018b), which are not conducive to photochemical production of O_3 (*Lu et al, 2018b; Tang et al., 2013*). The onset of the summer monsoon is also associated with strong air convergence and uplift, which is not favorable for the accumulation of O_3 and its precursors (*Lu et al, 2018b*).

North China is less influenced by the summer monsoon as suggested by the insignificant precipitation in summer (Fig. S7c). East China and South China are more affected as suggested by DNSMI values higher than 0.5 and more abundant precipitation (Fig. 5c and Fig. S7c). High temperature and stronger solar radiation in summer favor the photochemical production of O_3. As a result, O_3 concentrations in the NCP peak in summer, exhibiting an inverted V-shaped pattern (Fig. 4a). The YRD region is affected moderately by the summer monsoon, with DNSMI values greater than 0.6 and mean precipitation greater than 7mm/day (Fig. 5c and S7c). The upwind sources for the YRD in summer include both polluted (south China) and clean (ocean) regions. Thus, the inhibition of O_3 formation in the YRD due to the summer monsoon does not lead to the annual minima in summer. Because of the favorable weather conditions (increasing temperature and solar radiation, and low precipitation) in spring and autumn (Fig. S7d), the seasonality of O_3 in the YRD exhibits a bridge shape, consistent with previous observations within this region (*Tang et al., 2013*). In addition, southerly winds might bring O_3 and its precursors from the YRD region in summer (Fig. 5c), which is further quantified in Sect. 4.3. For India and the PRD region, the alternation of wind fields and precipitation begins as spring approaches (Fig. 5 and Fig. S7). As a result, O_3 concentrations decline in response to input of cleaner air from the ocean and more precipitation. As summer arrives, the intensity of the monsoon reaches its maximum (Fig. 5c and S7) and concentrations of O_3 in both India and South China decline to reach their annual minima (Fig. 4c and Fig. 4d). As wind direction changes over the east coast of China from summer to autumn, O_3 peaks in autumn in South China can be attributed also to the outflow of O_3 and its precursors from the NCP and YRD regions (Fig. 5d). This contribution is discussed further also in Sect. 4.3.

4.2 O_3 sensitivity to emissions from individual source sectors

O_3 in the troposphere is formed through complex nonlinear processes involving emissions of NO_x and VOCs from various anthropogenic, biogenic, and biomass burning sources. We illustrate in Fig. 6 the sensitivity of seasonal mean O_3 concentrations in both China and India to individual source sectors, patterns that offer important implications for seasonal O_3 control strategies in some highly polluted regions. The sensitivity is defined as the responses of O_3 concentration to the elimination of each source sector ($O_{3_{with\ all\ emissions}} - O_{3_{without\ each\ sector}}$). For China, summer O_3 formation is more sensitive to industrial sources than to other anthropogenic sources, including power, residential, and transport (Fig. 6c and Table 3). Emissions from the industrial sector are responsible for an enhancement of O_3 concentrations by more than 8 ppb in the NCP and YRD regions in summer (Fig. 6c and Table 3). Using a similar approach, *Li et al. (2017)* reported that the contribution to O_3 from industrial sources exceeded 30 μg/m^3 (~15 ppb) in highly industrialized areas, including Hebei, Shandong, Zhejiang, etc. during an episode in May. *Li et al. (2016)* concluded that the industrial sector plays the most important role for O_3 formation in Shanghai, accounting for more than 35% of observed concentrations. Adopting a source-oriented chemical transport model, *Wang et al., (2019)* demonstrated that the industrial source contributes 36%, 46%, and 29% to non-background O_3 in Beijing, Shanghai and Guangdong, respectively.

In the NCP and YRD regions, O_3 formation in winter, spring, and autumn reflects negative sensitivity to the transport and power sectors (Fig. 6 and Table 3). These two sectors dominate emissions of NO_x in China (*Li et al., 2017*). Removing these sectors would lead to increases in O_3 in VOC-limited regions of east China in winter, spring and fall (less biogenic emissions of VOCs in these seasons, *Fu et al., 2012*). The ratio of formaldehyde to reactive nitrogen ($HCHO/NO_y$) is widely used to determine the O_3 production sensitivity with critical value of 0.28 (*Sillman, 1995; Zhao et al., 2009*). Fig. S8 indicates that east China is VOCs-limited in winter, spring and fall. Urban regions in China are still VOC-limited (Fig. S8c, *Fu et al., 2012; Jin et al., 2017*) in summer, leading to negligible or negative sensitivity to the transport and power sectors as shown in Fig. 6g and Fig 6o. In other regions of east China, removing transport and power sources would lead to an increase in O_3 concentrations by about 4 ppb in summer. The negative sensitivity of O_3 to the transport and power sectors may be also caused by the

343 nighttime titration effects. In winter, daytime mean O_3 exhibit also negative sensitivity to
344 transportation sector, and similar distribution with daily mean O_3 sensitivity (Fig. S9a and S9b),
345 suggesting nighttime titration effects might not be the major reason in winter. However,
346 daytime mean and daily mean O_3 exhibit different patterns of sensitivity to transportation sector
347 in highly urbanized regions in summer, which could be related to nighttime titration effects. As
348 indicated in Fig. S10, O_3 sensitivity to transportation sector in Beijing is positive during the
349 day but negative during the night.
350 Including biogenic emissions results in an increase in summer mean O_3 concentrations by more
351 than 18 ppb in the NCP and YRD regions (Fig. 6s and Table 3). The large sensitivity of O_3 to
352 biogenic emissions is associated with the massive VOCs emitted from biosphere (Table S2).
353 The amount of biogenic VOCs is comparable to those emitted from all anthropogenic sectors
354 in China and greater than anthropogenic VOCs in India (Table S2). Using a similar approach,
355 *Li et al. (2018)* found that biogenic emissions contributed 8.2 ppb in urban Xi'an. Other source
356 apportionment studies indicate that the contribution of biogenic emissions to O_3 formation is
357 about 20% in China (*Li et al., 2016; Wang et al., 2019*). The enhancements due to biogenic
358 emissions are larger over south China during winter, and the significantly impacted regions
359 extend northwards in spring and autumn (Fig. 6q-6t). Biomass burning emissions lead to
360 relatively lower O_3 enhancements over China in winter, but they are responsible for an
361 appreciable contribution to O_3 pollution (~4 ppb) in east China in summer (Fig. 6w and Table
362 3). *Li et al. (2016)* suggested that biomass burning sources contribute about 4% to O_3 formation
363 in the YRD region in summer. The enhancement due to biomass burning estimated by *Lu et al.*
364 *(2019)* using a different model indicates lower values in east China.
365 For India, O_3 formation is most sensitive to the transport vehicle sector (~8 ppb) in all seasons
366 (Table 3), slightly higher than it is to the biogenic source (Fig. 6m-6p and Table 3). Among
367 other sectors, the sensitivity of O_3 formation to the residential sector is significant in winter as
368 residential sector emits the largest amount of NMVOCs (*Li et al., 2017*), while the influence
369 of biomass burning emissions is negligible.
370 To further address the issue of nighttime titration effects, we calculated also the sensitivity of
371 daytime O_3 formation in July to sectors, and we found that daytime O_3 in the NCP and YRD
372 are also most sensitive to industrial and biogenic emissions (Table 4). Among other

anthropogenic sectors, transportation emissions play important roles in the formation of daytime O_3 in China, followed by power generation emissions (Table 4).Our results highlight the importance of industrial sources and biogenic emissions in O_3 formation in east China, consistent with the conclusions of *Li et al.* (*2017*). The significance of other sectors demonstrated by *Li et al.* (*2017*) partly disagrees with the current findings. Conclusions from *Li et al. (2017)* rely on simulations of a one-week episode in May, while our results provide more information considering different seasons and different highly polluted regions.

4.3 O_3 contribution from individual source regions

The sensitivity of O_3 pollution to individual source sectors discussed in the previous section provides a quantitative understanding of the relative importance of individual source sectors. Additionally, information on the contribution of individual source regions to O_3 pollution should provide useful inputs for O_3 control strategies. Because of the large computational costs of sensitivity simulations, we employed the tagging method to examine contributions to O_3 pollution from individual source regions. Fig. 7 presents monthly mean concentrations of O_3 averaged over the NCP, YRD, PRD and India, with contributions from individual source regions.

The NCP region is influenced largely by sources outside China, especially in wintertime, which might be attributed to less local production and a longer O_3 lifetime in winter. In winter, sources outside China are responsible for more than 75% of O_3 formation in the NCP region. However, this contribution declines to about 50% as summer approaches. Using the tagged tracer method with a global chemical transport model, *Nagashima et al. (2010)* suggested that sources outside China contributed about 60% and 40% to surface O_3 in North China in spring and summer, respectively. Our estimate for the contributions of sources outside China in these two seasons suggests slightly higher values: 73% and 51% (Table 5). In summer, NCP local sources contribute about 31%, with additional 8% from Northwestern China.

For the YRD region, local emissions contribute 32% to O_3 formation in summer, but the contribution declines by 8% in spring and autumn (Table 5). The contribution of sources outside China decreases greatly in summer (46%), leading to a small summer O_3 trough. The source apportionment results in *Nagashima et al. (2010)* also indicated that the contribution of

sources outside China to O_3 in the Yangtze River Basin decreases significantly from spring to summer (44% to 30%). The relatively lower contribution from sources outside China is associated with the prevailing winds and cleaner air from the ocean in summer (Fig. 5c). In addition to local sources, we further identified the major source region for O_3 in the YRD region is the NCP in winter, spring and autumn (14%, 6% and 8%, respectively). In summer, the major source region of O_3 in the YRD region is Southeast China (10%). *Gao et al. (2016a)* concluded that YRD local emissions contribute 13.6%-20.6% to daytime O_3 under different wind conditions, and the contribution of super regional sources (Outside) ranges from 32 to 34% in May. In Hangzhou (a megacity within YRD), source apportionment results reveal that long-range transport contributes 36.5% to daily maximum O_3 with the overall contribution dominated by local sources (*Li et al., 2016*).

O_3 concentrations in the YRD region are influenced largely by the summer monsoon, and the prevailing winds from the ocean result in a minimum contribution from polluted regions. The estimated contribution of sources outside China declines to 46% in summer, which agrees well with the number 47% inferred from *Nagashima et al. (2010)*. *Li et al. (2012)* applied the OSAT tool in the CAMx model to apportion O_3 sources in south China, and they reported that super-regional sources contributed 55% and 71% to monthly mean O_3 in summer and autumn, respectively. They pointed out also that regional and local sources play more important roles in O_3 pollution episodes (*Li et al., 2002*). The contribution of local source peaks in summer (41%) exceeds the local contribution in the NCP and YRD regions. As discussed in Sect. 4.1, the outflow of O_3 and its precursors from the NCP and YRD regions might play important roles in peak autumn O_3 in the YRD (Fig. 5d), as wind direction switches from summer to autumn. We identified the major upwind regions for the PRD in autumn as YRD (11%) and Southeast China (10%). From summer to autumn, the contribution of YRD sources to the PRD increases from 2% to 11%. For India, O_3 concentrations are dominated by sources outside India, and sources in North India (Fig. 7d). In winter, sources outside India contribute 49%, while sources in North India contribute 38%.

We calculated also the contributions of sources in different regions to MDA8 O_3 concentrations, and we compared the results with contributions to daily mean O_3. As shown in Fig. 8, the contributions of sources in different regions do not exhibit a large difference for Beijing, except

433 that the local sources play a more important role in the formation of daytime O_3 in winter (Fig.
434 8a). Similarly, higher contributions of local sources to the formation of daytime O_3 are found
435 for Guangzhou in autumn, and for Shanghai in all seasons (Fig. 8). The contributions of sources
436 in different regions do not show a notable difference for New Delhi, India.
437 The estimated contributions of sources outside China to O_3 pollution in receptor regions exhibit
438 slightly higher values than the values inferred from studies using global models (*Nagashima et*
439 *al., 2010; Wang et al., 2011*). This might be related partly to the inconsistency between
440 simulations from the applied regional model and boundary conditions from another global
441 model. Global chemical transport models usually show better skills in simulating
442 transboundary pollution.
443

444 **5 Discussion and Summary**

445 In this study, we used a fully coupled regional meteorology-chemistry model with a horizontal
446 grid spacing of 60 km × 60 km to study the seasonality and characteristics of sources of O_3
447 pollution in highly polluted regions in both China and India. Both observations and model
448 results indicate that O_3 in the NCP, YRD, PRD, and in India display distinctive seasonal
449 features. Surface concentrations of O_3 peak in summer in the NCP, in spring in the YRD, in
450 autumn in the PRD and in winter in India. These distinct seasonal features for different regions
451 are linked to the intensity of the summer monsoon, to sources, and to atmospheric transport.
452 With confidence in the model's ability to reproduce the major features of O_3 pollution, we
453 examined the sensitivity of O_3 pollution to individual anthropogenic emission sectors, and to
454 emissions from biogenic sources and from burning of biomass. We found that production of O_3
455 in summer is more sensitive to industrial and biogenic sources than to other source sectors for
456 China, while the transportation and biogenic emissions are more important for all seasons in
457 India. For India, in addition to transportation, the residential sector also plays an important role
458 in winter when O_3 concentrations peak. These differences in conditions between China and
459 India suggest differences in control strategies on economic sectors should be implemented to
460 minimize resulting pollution.
461 Tagged simulations suggest that sources in east China play an important role in the formation

462 of the summer O_3 peak in the NCP, and sources from Northwest China should not be neglected
463 to control summer O_3 in the NCP. For the YRD region, prevailing winds and cleaner air from
464 the ocean in summer lead to reduced transport from polluted regions, and the major source
465 region in addition to local sources is Southeast China. For the PRD region, the upwind region
466 is replaced by contributions from polluted east China as autumn approaches, leading to an
467 autumn peak. The major upwind regions in autumn for the PRD are YRD (11%) and Southeast
468 China (10%). For India, sources in North India show larger contributions than sources in South
469 India.
470 The focus of our analysis is on the seasonality of O_3 pollution and its sources in both China
471 and India, with an emphasis on implications for O_3 control strategies. Most previous studies
472 focused on the analysis of episodes or monthly means for a region, while the current study
473 presents a more comprehensive picture. For the NCP region, O_3 concentrations peak in summer,
474 during which industrial sources should be given higher priority. Besides local sources in the
475 NCP, sources from Northwest China play also important roles. For the YRD region, O_3
476 concentrations in spring, summer and autumn are equally important, showing appreciable
477 sensitivity to the industrial sources. In addition to local sources, sources from the NCP should
478 be considered for control of O_3 in spring and autumn, while sources from Southeast China
479 should be considered in summer. For the PRD region, O_3 concentrations peak in spring and
480 autumn, during which reducing industrial and transportation sources could be more effective.
481 In both spring and autumn, sources from the YRD and Southeast China show appreciable
482 contributions to O_3 pollution in the PRD. For India, O_3 pollution is more serious in winter,
483 during which controlling residential and transport sources in North India could be more
484 effective.
485 However, uncertainties remain in the conclusions resulting from the assumptions and
486 methodology adopted in this study. The zero-out method is computationally inefficient. It is a
487 sensitivity method, and does not provide source contribution for nonlinear systems, as the sum
488 of impacts of all sources will not equal the total concentration (*Yarwood et al., 2007*). Although
489 there is no perfect source apportionment technique for nonlinear systems, reasonable method
490 that tracks mass contributions and accounts for chemical nonlinearity can provide additional
491 information in terms of the design of control strategies (*Yarwood et al., 2007*). In the tagging

method, photochemical indicator HCHO/NO_y with threshold of 0.28 (*Sillman, 1995*) was used to determine NO_x- or VOC-limited, which can also result in uncertainties in the results. There are several other indicators have been proposed to indicate photochemical sensitivity, including O_3/NO_x, O_3/NO_y, etc. However, the robustness of these indicators can vary with ambient conditions and locations (*Andreani-Aksoyoglu et al., 2001*). *Zhang et al. (2009)* recommended using multiple indicators rather than a single one to reduce uncertainties. *Wang et al. (2019)* suggested that the use of a single threshold for these indicators is insufficient, as O_3 can be sensitive to both NO_x and VOCs. A three-regime O_3 attribution technique was developed by *Wang et al. (2019)* to address this problem. Additionally, although comparisons are shown for daytime mean and daily mean, most conclusions in this study are based on seasonal mean (both daytime and nighttime) O_3 while many previous studies investigate sources of 8-h or daily maximum O_3. As illustrated in *Li et al. (2016)*, the dominant contribution to nighttime O_3 is associated with long-range transport. All of these factors contribute to uncertainties in the results of source apportionment, but should not downplay the significance of current findings in terms of policy implications.

2 tables and 10 figures are listed in the supplement.

Author contribution

MG and MBM designed the study; MG performed model simulations and analyzed the data with the help from JG, BZ, RK, XL, SS, YZ, BJ, PW, PS; GB, JH, QY, HZ provided measurements. MG and MBM wrote the paper with inputs from all other authors.

Data availability

The measurements and model simulations data can be accessed through contacting the corresponding authors.

Competing interests

The authors declare that they have no conflict of interests.

Acknowledgement

This work is supported by the special fund of Key Laboratory for Aerosol-Cloud-Precipitation of China Meteorological Administration, Nanjing University of Information Science and Technology (KDW1901), Harvard Global Institute, special fund of State Key Joint Laboratory of Environment Simulation and Pollution Control (19K03ESPCT), the Natural Science Foundation of Guangdong Province (no. 2019A1515011633), National Natural Science Foundation of China Major Research Plan (Integrated Project) (NSFC91843301), and the National Key Research and Development Program-Cooperation on Scientific and Technological Innovation in Hong Kong, Macau and Taiwan (2017YFE0191000).

Reference

Andreani-Aksoyoglu, S., Lu, C. H., Keller, J., Prevot, A. S. H., and Chang, J. S.: Variability of indicator values for ozone production sensitivity: a model study in Switzerland and San Joaquin Valley (California), Atmos. Environ., 35, 5593–5604, doi:10.1016/S1352-2310(01)00278-3, 2001.

Beig, G., Gunthe, S. and Jadhav, D. B.: Simultaneous measurements of ozone and its precursors on a diurnal scale at a semi urban site in India, J. Atmos. Chem., 57(3), 239–253, doi:10.1007/s10874-007-9068-8, 2007.

Beig G., GAW Report No. 217, System of Air Quality Forecasting and Research (SAFAR-INDIA), World Meteorological Organization, 2015.

Chameides, W.L., Kasibhatla, P.S., Yienger, J., Levy II, H.: Growth of Continental-scale Metro-Agro-Plexes, Regional Ozone Pollution, and World Food Production, Science (80-.)., 264(APRIL), 1994.

Cheng, N., Li, Y., Zhang, D., Chen, T., Sun, F., Chen, C. and Meng, F.: Characteristics of Ground Ozone Concentration over Beijing from 2004 to 2015: Trends, Transport, and Effects of Reductions, Atmos. Chem. Phys. Discuss., 1(x), 1–21, doi:10.5194/acp-2016-508, 2016.

De Smedt, I., Stavrakou, T., Mller, J. F., Van Der A, R. J. and Van Roozendael, M.: Trend detection in satellite observations of formaldehyde tropospheric columns, Geophys. Res. Lett., 37(18), doi:10.1029/2010GL044245, 2010.

Duncan, B.N., Lamsal, L.N., Thompson, A.M., Yoshida, Y., Lu, Z., Streets, D.G., Hurwitz, M.M. and Pickering, K.E.: A space-based, high-resolution view of notable changes in urban NOx pollution around the world (2005–2014), J. Geophys. Res. Atmos., 121(2), pp.976-996, 2016.

Emmons, L. K., Walters, S., Hess, P. G., Lamarque, J.-F., Pfister, G. G., Fillmore, D., Granier, C., Guenther, a., Kinnison, D., Laepple, T., Orlando, J., Tie, X., Tyndall, G., Wiedinmyer, C., Baughcum, S. L. and Kloster, S.: Description and evaluation of the Model for Ozone and Related chemical Tracers, version 4 (MOZART-4), Geosci. Model Dev., 3(1), 43–67, doi:10.5194/gmd-3-43-2010, 2010.

Fu, J. S., Dong, X., Gao, Y., Wong, D. C. and Lam, Y. F.: Sensitivity and linearity analysis of ozone in East Asia: The effects of domestic emission and intercontinental transport, J. Air Waste Manage. Assoc., 62(March 2015), 1102–1114, doi:10.1080/10962247.2012.699014, 2012.

Gao, J., Zhu, B., Xiao, H., Kang, H., Hou, X. and Shao, P.: A case study of surface ozone source apportionment during a high concentration episode, under frequent shifting wind conditions over the Yangtze River Delta, China, Sci. Total Environ., 544, 853–863, doi:10.1016/j.scitotenv.2015.12.039, 2016a.

Gao, M., Carmichael, G. R., Wang, Y., Saide, P. E., Yu, M., Xin, J., Liu, Z. and Wang, Z.: Modeling study of the 2010 regional haze event in the North China Plain, Atmos. Chem. Phys., 16(3), 1673–1691, doi:10.5194/acp-16-1673-2016, 2016b.

Gao, M., Saide, P. E., Xin, J., Wang, Y., Liu, Z., Wang, Y., Wang, Z., Pagowski, M., Guttikunda, S. K. and Carmichael, G. R.: Estimates of Health Impacts and Radiative Forcing in Winter Haze in Eastern China through Constraints of Surface PM2.5 Predictions, Environ. Sci. Technol., 51(4), 2178–2185, doi:10.1021/acs.est.6b03745, 2017b.

Gao, M., Han, Z., Liu, Z., Li, M., Xin, J., Tao, Z., Li, J., Kang, J. E., Huang, K., Dong, X., Zhuang, B., Li, S., Ge, B., Wu, Q., Cheng, Y., Wang, Y., Lee, H. J., Kim, C. H., Fu, J. S., Wang, T., Chin, M., Woo, J. H., Zhang, Q., Wang, Z. and Carmichael, G. R.: Air quality and climate change, Topic 3 of the Model Inter-Comparison Study for Asia Phase III (MICS-Asia III) - Part 1: Overview and model evaluation, Atmos. Chem. Phys., 18(7), 4859–4884, doi:10.5194/acp-18-4859-2018, 2018.

Ghude, S. D., Jena, C., Chate, D.M., Beig, G., Pfister, G.G., Kumar, R., Ramanathan, V.: Reductions in India's crop yield due to ozone, Geophys. Res. Lett., 41, 5685–5691, doi:10.1002/2014GL060930.Received, 2014.

Ghude, S. D., Jain, S. L., Arya, B. C., Beig, G., Ahammed, Y. N., Kumar, A. and Tyagi, B.: Ozone in ambient air at a tropical megacity, Delhi: Characteristics, trends and cumulative ozone exposure indices, J. Atmos. Chem., 60(3), 237–252, doi:10.1007/s10874-009-9119-4, 2008.

Giglio, L., Randerson, J. T. and Van Der Werf, G. R.: Analysis of daily, monthly, and annual burned area using the fourth-generation global fire emissions database (GFED4), J. Geophys. Res. Biogeosciences, 118(1), 317–328, doi:10.1002/jgrg.20042, 2013.

Grell, G. a., Peckham, S. E., Schmitz, R., McKeen, S. a., Frost, G., Skamarock, W. C. and Eder, B.:

Fully coupled “online” chemistry within the WRF model, Atmos. Environ., 39(37), 6957–6975, doi:10.1016/j.atmosenv.2005.04.027, 2005.

Guenther, A. B., Jiang, X., Heald, C. L., Sakulyanontvittaya, T., Duhl, T., Emmons, L. K. and Wang, X.: The model of emissions of gases and aerosols from nature version 2.1 (MEGAN2.1): An extended and updated framework for modeling biogenic emissions, Geosci. Model Dev., 5(6), 1471–1492, doi:10.5194/gmd-5-1471-2012, 2012.

Hakim, Z. Q., Archer-Nicholls, S., Beig, G., Folberth, G. A., Sudo, K., Luke Abraham, N., Ghude, S., Henze, D. K. and Archibald, A. T.: Evaluation of tropospheric ozone and ozone precursors in simulations from the HTAPII and CCMI model intercomparisons-A focus on the Indian subcontinent, Atmos. Chem. Phys., 19(9), 6437–6458, doi:10.5194/acp-19-6437-2019, 2019.

Hilboll, A., Richter, A. and Burrows, J. P.: Long-term changes of tropospheric NO2 over megacities derived from multiple satellite instruments, Atmos. Chem. Phys., 13(8), 4145–4169, doi:10.5194/acp-13-4145-2013, 2013.

Hu, J., Chen, J., Ying, Q. and Zhang, H.: One-year simulation of ozone and particulate matter in China using WRF/CMAQ modeling system, Atmos. Chem. Phys., 16(16), 10333–10350, doi:10.5194/acp-16-10333-2016, 2016.

Jin, X., Fiore, A. M., Murray, L. T., Valin, L. C., Lamsal, L. N., Duncan, B., Folkert Boersma, K., De Smedt, I., Abad, G. G., Chance, K. and Tonnesen, G. S.: Evaluating a Space-Based Indicator of Surface Ozone-NOx-VOC Sensitivity Over Midlatitude Source Regions and Application to Decadal Trends, J. Geophys. Res. Atmos., 122(19), 10439–10461, doi:10.1002/2017JD026720, 2017.

Kurokawa, J., Ohara, T., Morikawa, T., Hanayama, S., Janssens-Maenhout, G., Fukui, T., Kawashima, K. and Akimoto, H.: Emissions of air pollutants and greenhouse gases over Asian regions during 2000-2008: Regional Emission inventory in ASia (REAS) version 2, Atmos. Chem. Phys., 13(21), 11019–11058, doi:10.5194/acp-13-11019-2013, 2013.

Lal, S., Naja, M. and Subbaraya, B. H.: Seasonal variations in surface ozone and its precursors over an urban site in India, Atmos. Environ., 34(17), 2713–2724, doi:10.1016/S1352-2310(99)00510-5, 2000.

Li, J., Wang, Z., Akimoto, H., Yamaji, K., Takigawa, M., Pochanart, P., Liu, Y., Tanimoto, H. and Kanaya, Y.: Near-ground ozone source attributions and outflow in Central Eastern China during MTX2006, Atmos. Chem. Phys., 8(24), 7335–7351, doi:10.5194/acp-8-7335-2008, 2008.

Li, G., Bei, N., Cao, J., Wu, J., Long, X., Feng, T., Dai, W., Liu, S., Zhang, Q., and Tie, X.: Widespread and persistent ozone pollution in eastern China during the non-winter season of 2015: observations and source attributions, Atmos. Chem. Phys., 17, 2759–2774, https://doi.org/10.5194/acp-17-2759-2017, 2017.

649
650Li, J. and Zeng, Q.: A new monsoon index and the geographical distribution of the global monsoons,
651 Adv. Atmos. Sci., 20(2), 299–302, 2003.
652
653Li, J., Wang, Z., Akimoto, H., Yamaji, K., Takigawa, M., Pochanart, P., Liu, Y., Tanimoto, H. and
654 Kanaya, Y.: Near-ground ozone source attributions and outflow in central eastern China during
655 MTX2006, Atmos. Chem. Phys., 8(24), pp.7335-7351, 2008.
656
657Li, K., Jacob, D. J., Liao, H., Shen, L., Zhang, Q. and Bates, K. H.: Anthropogenic drivers of 2013–
658 2017 trends in summer surface ozone in China, Proc. Natl. Acad. Sci. U. S. A., 116(2), 422–
659 427, doi:10.1073/pnas.1812168116, 2019.
660
661Li, L. Y. and Xie, S. D.: Historical variations of biogenic volatile organic compound emission
662 inventories in China, 1981-2003, Atmos. Environ., 95, 185–196,
663 doi:10.1016/j.atmosenv.2014.06.033, 2014.
664
665Li, L., An, J. Y., Shi, Y. Y., Zhou, M., Yan, R. S., Huang, C., Wang, H. L., Lou, S. R., Wang, Q., Lu,
666 Q. and Wu, J.: Source apportionment of surface ozone in the Yangtze River Delta, China in the
667 summer of 2013, Atmos. Environ., 144, 194–207, doi:10.1016/j.atmosenv.2016.08.076, 2016.
668
669Li, M., Zhang, Q., Streets, D. G., He, K. B., Cheng, Y. F., Emmons, L. K., Huo, H., Kang, S. C.,
670 Lu, Z., Shao, M., Su, H., Yu, X. and Zhang, Y.: Mapping Asian anthropogenic emissions of
671 non-methane volatile organic compounds to multiple chemical mechanisms, Atmos. Chem.
672 Phys., 14(11), 5617–5638, doi:10.5194/acp-14-5617-2014, 2014.
673
674Li, M., Zhang, Q., Kurokawa, J. I., Woo, J. H., He, K., Lu, Z., Ohara, T., Song, Y., Streets, D. G.,
675 Carmichael, G. R., Cheng, Y., Hong, C., Huo, H., Jiang, X., Kang, S., Liu, F., Su, H. and Zheng,
676 B.: MIX: A mosaic Asian anthropogenic emission inventory under the international
677 collaboration framework of the MICS-Asia and HTAP, Atmos. Chem. Phys., 17(2), 935–963,
678 doi:10.5194/acp-17-935-2017, 2017.
679
680Li, N., He, Q., Greenberg, J., Guenther, A., Li, J., Cao, J., Wang, J., Liao, H., Wang, Q. and Zhang,
681 Q.: Impacts of biogenic and anthropogenic emissions on summertime ozone formation in the
682 Guanzhong Basin, China, Atmos. Chem. Phys., 18(10), 7489–7507, doi:10.5194/acp-18-7489-
683 2018, 2018.
684
685Li, Y., Lau, A. K. H., Fung, J. C. H., Zheng, J. Y., Zhong, L. J. and Louie, P. K. K.: Ozone source
686 apportionment (OSAT) to differentiate local regional and super-regional source contributions
687 in the Pearl River Delta region, China, J. Geophys. Res. Atmos., 117(15), 1–18,
688 doi:10.1029/2011JD017340, 2012.
689
690Lu, X., Hong, J., Zhang, L., Cooper, O. R., Schultz, M. G., Xu, X., Wang, T., Gao, M., Zhao, Y. and
691 Zhang, Y.: Severe Surface Ozone Pollution in China: A Global Perspective, Environ. Sci.
692 Technol. Lett., 5(8), 487–494, doi:10.1021/acs.estlett.8b00366, 2018a.

693
694Lu, X., Zhang, L., Liu, X., Gao, M., Zhao, Y. and Shao, J.: Lower tropospheric ozone over India
695 and its linkage to the South Asian monsoon, Atmos. Chem. Phys., 18(5), 3101–3118,
696 doi:10.5194/acp-18-3101-2018, 2018b.
697
698Lu, X., Zhang, L., Chen, Y., Zhou, M., Zheng, B., Li, K., Liu, Y., Lin, J., Fu, T.-M., and Zhang, Q.:
699 Exploring 2016–2017 surface ozone pollution over China: source contributions and
700 meteorological influences, Atmos. Chem. Phys., 19, 8339–8361, https://doi.org/10.5194/acp-
701 19-8339-2019, 2019.
702
703Ma, Z., Xu, J., Quan, W., Zhang, Z., Lin, W. and Xu, X.: Significant increase of surface ozone at a
704 rural site, north of eastern China, Atmos. Chem. Phys., 16(6), 3969–3977, doi:10.5194/acp-16-
705 3969-2016, 2016.
706
707Malley, C.: Tropospheric Ozone Assessment Report: Present-day tropospheric ozone distribution
708 and trends relevant to vegetation. Elementa: Science of the Anthropocene, 2018.
709
710Nagashima, T., Ohara, T., Sudo, K. and Akimoto, H.: The relative importance of various source
711 regions on East Asian surface ozone, Atmos. Chem. Phys., 10(22), 11305–11322,
712 doi:10.5194/acp-10-11305-2010, 2010.
713
714NCEP, National Weather Service, NOAA & U.S. Department of Commerce. NCEP Final (FNL)
715 Operational Model Global Tropospheric Analyses, continuing from July 1999.
716 https://doi.org/10.5065/D6M043C6 (Research Data Archive at the National Center for
717 Atmospheric Research, Computational and Information Systems Laboratory, 2000).
718
719Ohara, T., Akimoto, H., Kurokawa, J., Horii, N., Yamaji, K., Yan, X. and Hayasaka, T.: An Asian
720 emission inventory of anthropogenic emission sources for the period 1980-2020, Atmos. Chem.
721 Phys., 7(16), 4419–4444, doi:10.5194/acp-7-4419-2007, 2007.
722
723Pachauri, R.K. and Reisinger, A.: IPCC fourth assessment report. IPCC, Geneva, p.2007, 2007.
724
725Saraf, N. and Beig, G.: Long-term trends in tropospheric ozone over the Indian tropical region,
726 Geophys. Res. Lett., 31(5), n/a-n/a, doi:10.1029/2003gl018516, 2004.
727
728Sharma, A., Ojha, N., Pozzer, A., Mar, K. A., Beig, G., Lelieveld, J., and Gunthe, S. S.: WRF-Chem
729 simulated surface ozone over south Asia during the pre-monsoon: effects of emission
730 inventories and chemical mechanisms, Atmos. Chem. Phys., 17, 14393–14413,
731 https://doi.org/10.5194/acp-17-14393-2017, 2017.
732Sillman, S.: The use of NOy, H2O2, and HNO3as indicators for ozone-NOx- hydrocarbon
733 sensitivity in urban locations, J. Geophys. Res., 100(D7), 175–188, 1995.
734
735Stavrakou, T., Müller, J. F., De Smedt, I., Van Roozendael, M., Van Der Werf, G. R., Giglio, L. and
736 Guenther, A.: Evaluating the performance of pyrogenic and biogenic emission inventories

against one decade of space-based formaldehyde columns, Atmos. Chem. Phys., 9(3), 1037–1060, doi:10.5194/acp-9-1037-2009, 2009.

Strode, S.A., Duncan, B.N., Yegorova, E.A., Kouatchou, J., Ziemke, J.R. and Douglass, A.R.: Implications of carbon monoxide bias for methane lifetime and atmospheric composition in chemistry climate models. Atmospheric chemistry and physics, 15(20), pp.11789-11805, 2015.

Sun, L., Xue, L., Wang, Y., Li, L., Lin, J., Ni, R., Yan, Y., Chen, L., Li, J., Zhang, Q. and Wang, W.: Impacts of meteorology and emissions on summertime surface ozone increases over central eastern China between 2003 and 2015, Atmos. Chem. Phys., 19(3), 1455–1469, doi:10.5194/acp-19-1455-2019, 2019.

Tang, H., Liu, G., Zhu, J., Han, Y. and Kobayashi, K.: Seasonal variations in surface ozone as influenced by Asian summer monsoon and biomass burning in agricultural fields of the northern Yangtze River Delta, Atmos. Res., 122, 67–76, doi:10.1016/j.atmosres.2012.10.030, 2013.

Wang, B., Wu, R. and Lau, K. M.: Interannual variability of the asian summer monsoon: Contrasts between the Indian and the Western North Pacific-East Asian monsoons, J. Clim., 14(20), 4073–4090, doi:10.1175/1520-0442(2001)014, 2001.

Wang, P., Chen, Y., Hu, J., Zhang, H. and Ying, Q.: Source apportionment of summertime ozone in China using a source-oriented chemical transport model, Atmos. Environ., 211(May), 79–90, doi:10.1016/j.atmosenv.2019.05.006, 2019.

Wang, T., Ding, A., Gao, J. and Wu, W. S.: Strong ozone production in urban plumes from Beijing, China, Geophys. Res. Lett., 33(21), doi:10.1029/2006GL027689, 2006.

Wang, T., Xue, L., Brimblecombe, P., Lam, Y. F., Li, L. and Zhang, L.: Ozone pollution in China: A review of concentrations, meteorological influences, chemical precursors, and effects, Sci. Total Environ., 575, 1582–1596, doi:10.1016/j.scitotenv.2016.10.081, 2017.

Wang, Y., Zhang, Y., Hao, J. and Luo, M.: Seasonal and spatial variability of surface ozone over China: Contributions from background and domestic pollution, Atmos. Chem. Phys., 11(7), 3511–3525, doi:10.5194/acp-11-3511-2011, 2011.

Wei, W., Wang, S., Hao, J. and Cheng, S.: Projection of anthropogenic volatile organic compounds (VOCs) emissions in China for the period 2010-2020, Atmos. Environ., 45(38), 6863–6871, doi:10.1016/j.atmosenv.2011.01.013, 2011.

Xu, X., Lin, W., Wang, T., Yan, P., Tang, J., Meng, Z. and Wang, Y.: Long-term trend of surface ozone at a regional background station in eastern China 1991-2006: Enhanced variability, Atmos. Chem. Phys., 8(10), 2595–2607, doi:10.5194/acp-8-2595-2008, 2008.

781 Yarwood, G., Morris, R.E., Yocke, M.A., Hogo, H. and Chico, T.: Development of a methodology
782 for source apportionment of ozone concentration estimates from a photochemical grid
783 model. AIR & WASTE MANAGEMENT ASSOCIATION, PITTSBURGH, PA
784 15222(USA).[np], 1996.
785
786 Yarwood, G., Morris, R. E., and Wilson, G. M.: Particulate matter source apportionment technology
787 (PSAT) in the CAMx photochemical grid model, Air Pollution Modeling and Its Application
788 XVII, 17, 478–492, https://doi.org/10.1007/978-0-387- 68854-1_52, 2007.
789
790 Zaveri, R. a., Easter, R. C., Fast, J. D. and Peters, L. K.: Model for Simulating Aerosol Interactions
791 and Chemistry (MOSAIC), J. Geophys. Res., 113(D13), D13204, doi:10.1029/2007JD008782,
792 2008.
793
794 Zaveri, R. a. and Peters, L. K.: A new lumped structure photochemical mechanism for large-scale
795 applications, J. Geophys. Res., 104(D23), 30387, doi:10.1029/1999JD900876, 1999.
796
797 Zhang, Y., Wen, X.-Y., Wang, K., Vijayaraghavan, K., and Jacobson, M. Z.: Probing into regional
798 O3 and particulate matter pollution in the United States: 2. An examination of formation
799 mechanisms through a process analysis technique and sensitivity study, J. Geophys. Res., 114,
800 D22305, doi:10.1029/2009JD011900, 2009.
801
802 Zhao, C., Wang, Y., and Zeng, T.: East China plains: A “basin” of ozone pollution, Environ. Sci.
803 Technol., 43, 1911–1915, 2009.
804 Zheng, B., Tong, D., Li, M., Liu, F., Hong, C., Geng, G., Li, H., Li, X., Peng, L., Qi, J., Yan, L.,
805 Zhang, Y., Zhao, H., Zheng, Y., He, K. and Zhang, Q.: Trends in China’s anthropogenic
806 emissions since 2010 as the consequence of clean air actions, Atmos. Chem. Phys., 18(19),
807 14095–14111, doi:10.5194/acp-18-14095-2018, 2018.
808
809
810
811
812
813
814
815
816
817
818
819

820 Table 1. Descriptions of simulations

Simulations	Descriptions
Control	Anthropogenic, biogenic and fire emissions are considered;
Industrial	Same as control except industry sector in anthropogenic emissions is excluded;
Residential	Same as control except residential sector in anthropogenic emissions is excluded;
Transportation	Same as control except transportation sector in anthropogenic emissions is excluded;
Power	Same as control except power sector in anthropogenic emissions is excluded;
Biogenic	Same as control except biogenic emissions are excluded;
Fire	Same as control except fire emissions are excluded;

821

822

823 Table 2 Model evaluation statistics

Regions	NCP	YRD	PRD	India
Mean Bias	-3.8	-1.8	3.1	-2.0
Root Mean Square Error	6.4	5.5	7.9	4.4
Normalized Mean Bias	-13.3%	-6.2%	10.7%	-5.6%
Normalized Mean Error	18.7%	14.9%	21.2%	11.1%
R	0.98	0.96	0.84	0.91

824

825

826

827

828

829

830

831 Table 3. Sensitivity of seasonal O_3 to emission sectors for different regions (ppb)

Sectors	Seasons	NCP	YRD	PRD	India
Industry	Winter	-4.1	-1.5	4.5	2.1
	Spring	-0.3	3.8	6.5	1.7
	Summer	8.3	8.3	4.7	1.6
	Autumn	-1.4	1.7	7.1	2.1
Power	Winter	-5.6	-7.5	-1.2	1.7
	Spring	-3.2	-2.2	2.2	2.3
	Summer	2.7	2.9	3.3	1.9
	Autumn	-3.3	-3.3	2.1	2.4
Residential	Winter	5.1	7.7	6.6	4.2
	Spring	2.4	2.5	1.9	2.4
	Summer	2.5	1.4	1.1	2.2
	Autumn	2.2	2.2	1.6	3.2
Transport	Winter	-8.5	-8.0	0.2	7.6
	Spring	-3.7	-1.5	3.4	7.9
	Summer	2.8	4.0	3.6	6.7
	Autumn	-4.3	-3.3	3.0	8.9
Biogenic	Winter	0.3	1.0	3.8	4.8
	Spring	4.3	6.6	7.5	5.6
	Summer	19.2	18.5	9.4	5.7
	Autumn	5.7	6.5	11.4	8.0
Fire	Winter	0.1	0.2	2.3	0.6
	Spring	1.1	1.8	2.6	1.1
	Summer	3.8	4.0	1.2	0.2
	Autumn	1.2	1.4	1.9	0.5

832

833

834

835 Table 4. Sensitivity of summer (July) daytime O_3 to emission sectors for different regions

836 (ppb)

Sectors	NCP	YRD	PRD	India
Industry	19.9	14.3	7.1	2.3
Power	6.1	7.0	4.9	2.7
Residential	4.1	1.9	1.6	3.3
Transport	8.9	9.2	5.9	10.0
Biogenic	28.7	28.9	12.0	7.6
Fire	1.4	0.8	0.3	0.1

837

838 Table 5. Long range transport, local, and regional source contributions for seasonal mean O3

839 for different regions

	NCP	YRD	PRD	India
Winter	Outside: 81%	Outside:51%	Outside: 44%	Outside: 49%
	Local: 12%	Local: 26%	Local: 13%	N India: 35%
	NW China: 6%	NCP: 14%	YRD: 13%	S India: 16%
Spring	Outside: 73%	Outside:59%	Outside: 48%	Outside: 58%
	Local: 17%	Local: 24%	Local: 27%	N India: 28%
	NW China: 5%	NCP: 6%	YRD: 7%	S India: 14%
			SE China: 6%	
Summer	Outside: 51%	Outside:46%	Outside: 46%	Outside: 45%
	Local: 31%	Local: 32%	Local: 41%	N India: 38%
	NW China: 8%	SE China: 10%	SE China: 4%	S India: 17%
Autumn	Outside: 69%	Outside:61%	Outside: 50%	Outside: 42%
	Local: 21%	Local: 24%	Local: 15%	N India: 41%
	NW China: 7%	NCP: 8%	YRD: 11%	S India: 17%
			SE China: 10%	

840 (Outside sources represent sources outside China for the discussed three regions in China, and sources outside

India for India, including also transport from upper boundary of the model; NCP: Beijing, Tianjin, Hebei, Shandong, and Henan; YRD: Anhui, Jiangsu, Shanghai and Zhejiang; SE China: Jiangxi, Fujian and Taiwan; Central China: Hunan and Hubei; South China: Guangxi and Hainan)

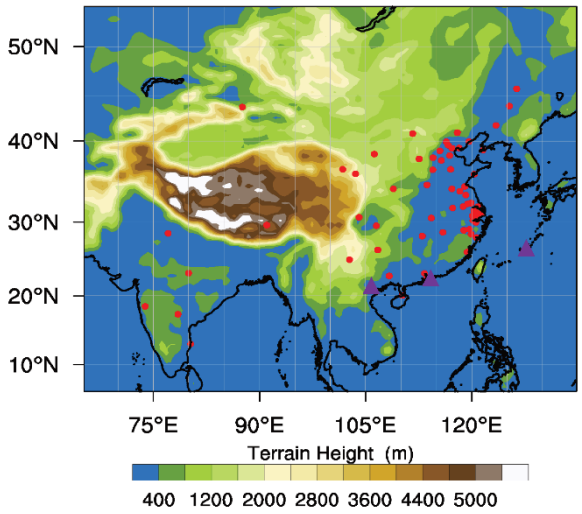

Fig. 1. WRF-Chem domain setting with terrain height and the locations of surface ozone observations marked by solid red circles. Purple solid triangles mark the location of ozonesonde observations.

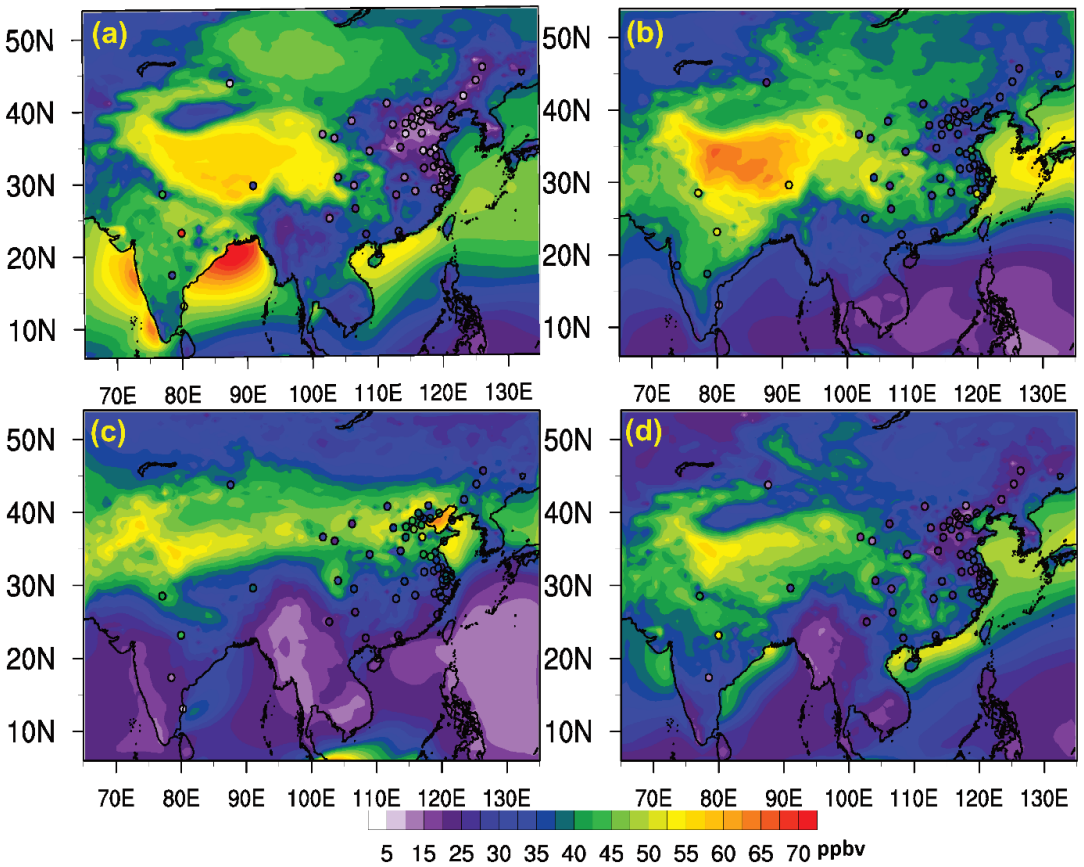

Fig. 2. Spatial distribution of simulated and observed seasonal mean ozone concentrations for Winter (a), Spring (b), Summer (c) and Fall (d).

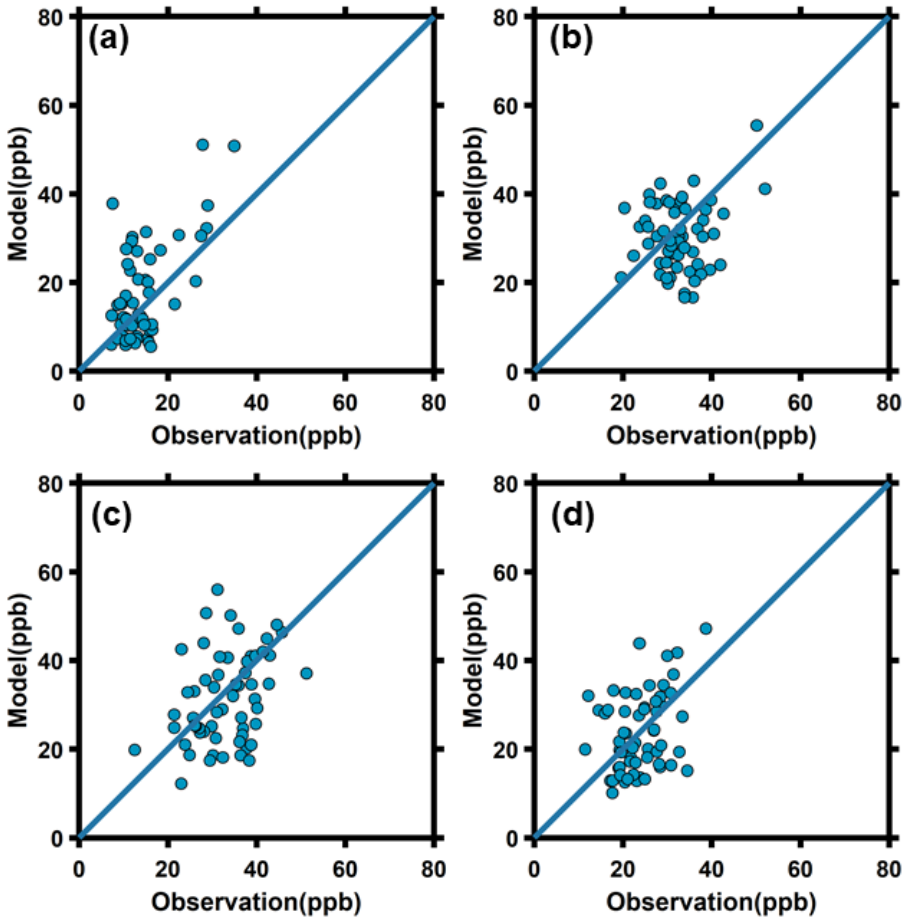

Fig. 3. Scatter plot of simulated and observed seasonal mean ozone concentrations for Winter (a), Spring (b), Summer (c) and Fall (d).

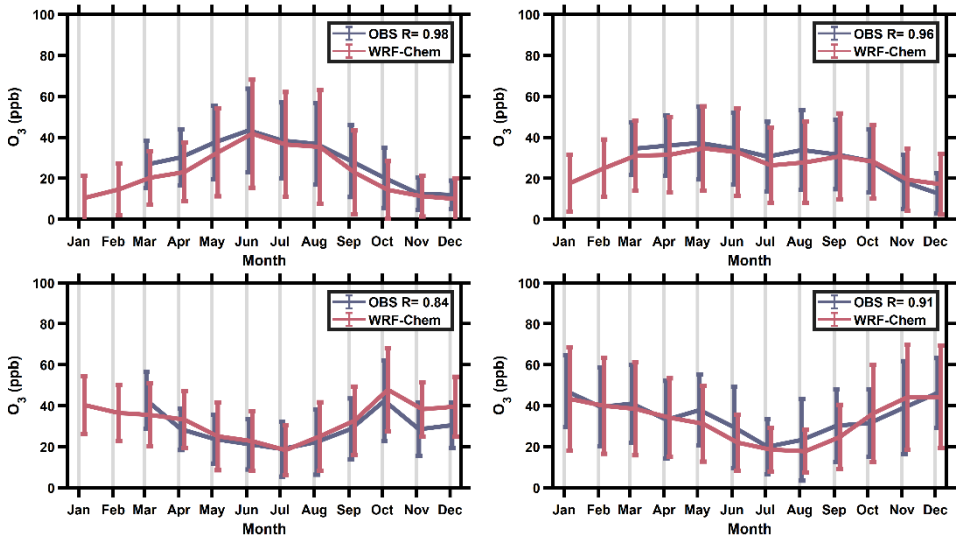

Fig. 4. Observed and simulated monthly mean O_3 concentrations averaged for the North China Plain (NCP) (a), Yangtze River Delta (YRD) (b), Pearl River Delta (PRD) (c), and India (d).

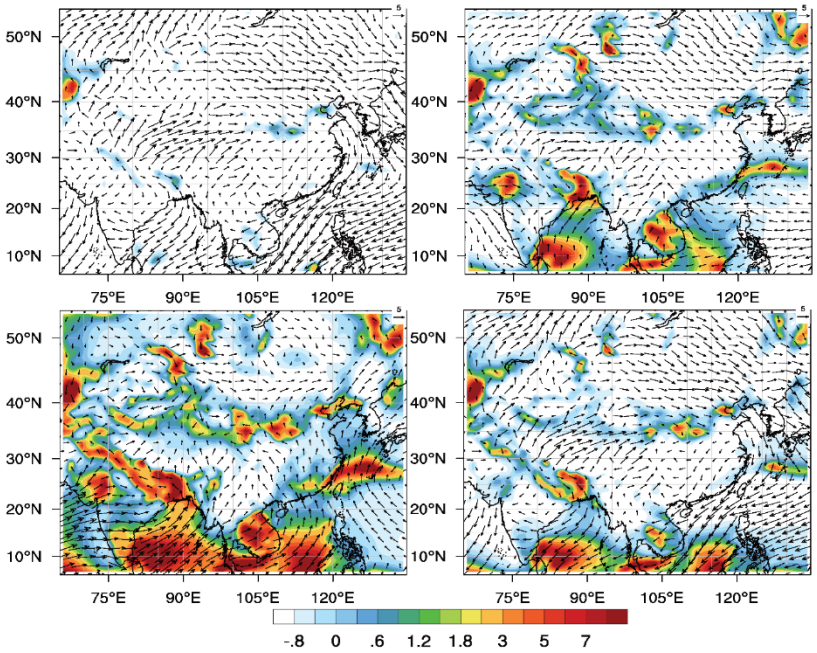

Fig. 5. Modeled mean near surface wind fields (winds at 10 meters above ground) and the monsoon index in the boundary layer (0-1.5km) for winter (December, January, and February, a), spring (March, April, and May, b), summer (June, July and August, c), and autumn (September, October, and November, d).

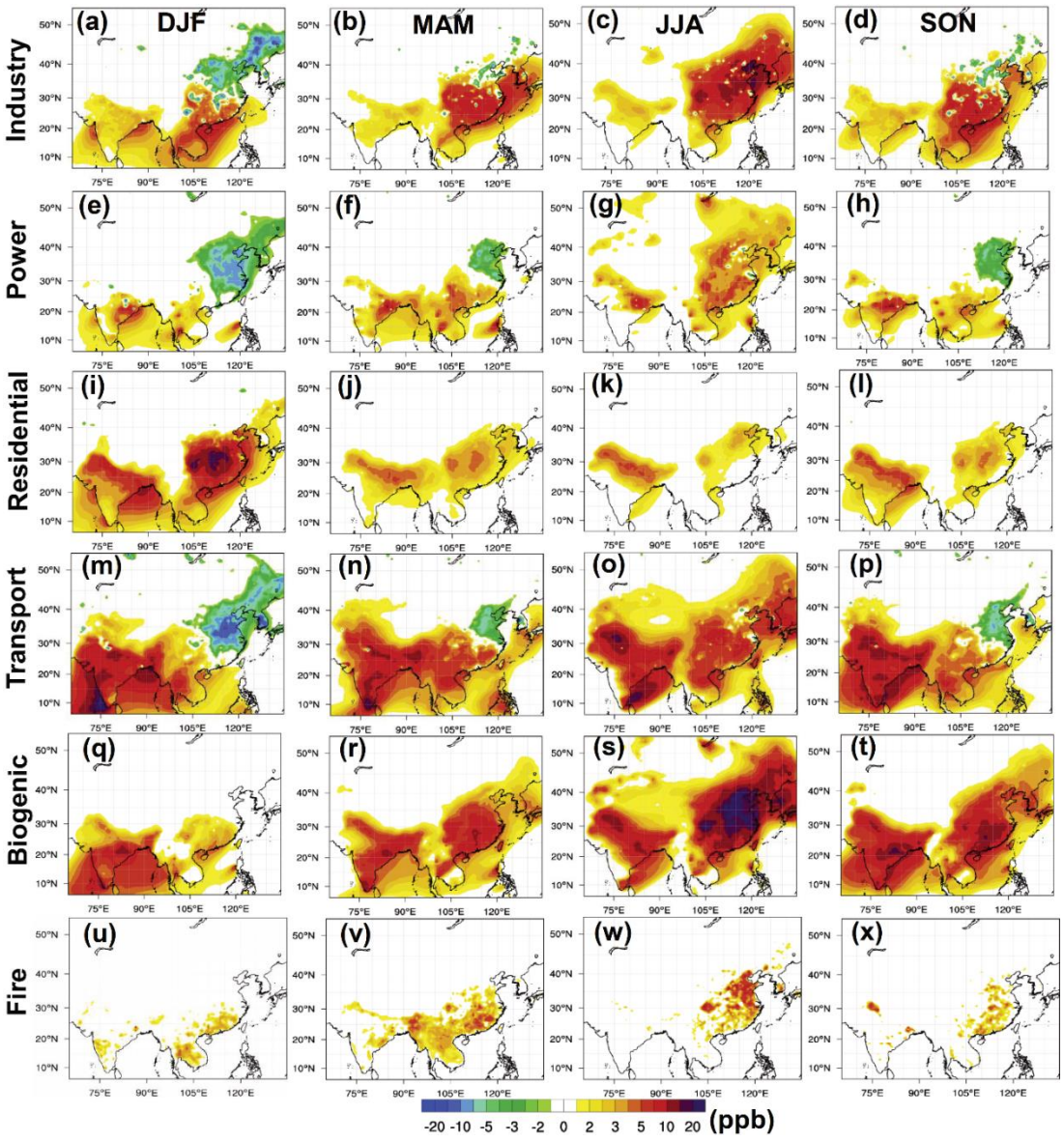

Fig. 6. Distributions of the contributions to near-surface ozone averaged for winter, spring, summer and autumn from industry (a-d), power, (e-h), residential (i-l), transport (m-p), biogenic (q-t) and fire/biomass burning (u-x) emissions.

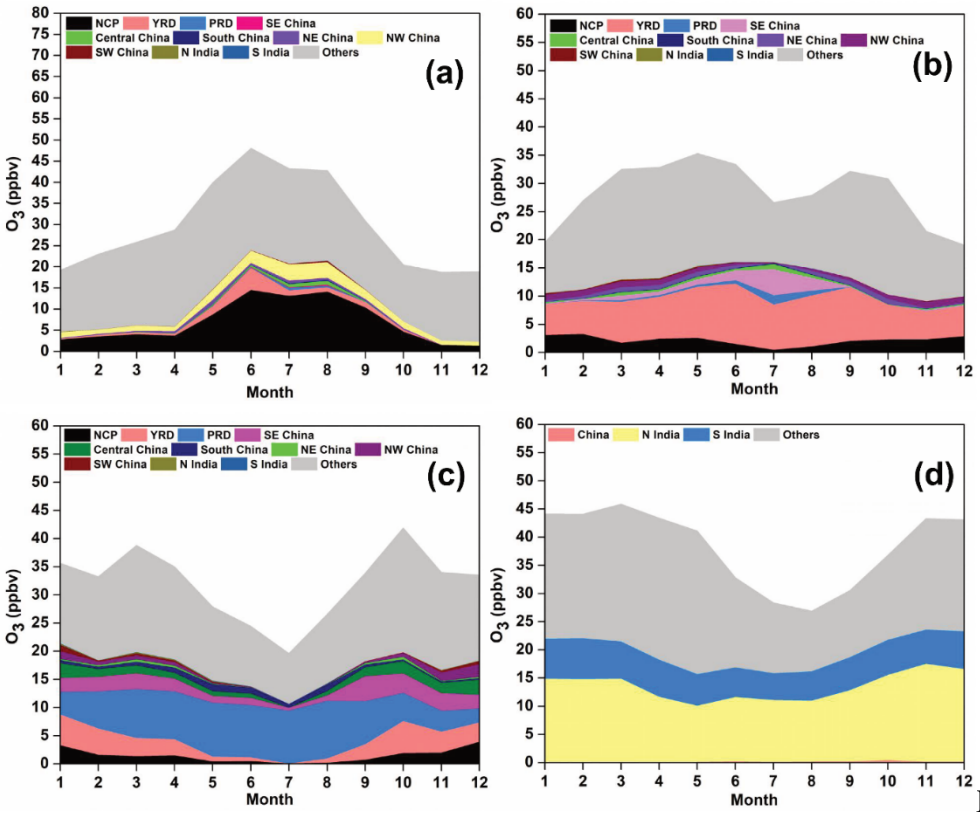

Fig. 7. Contributions to monthly mean ozone in NCP (a), YRD (b), PRD (c), and India (d) from different source regions (NCP: Beijing, Tianjin, Hebei, Shandong, and Henan; YRD: Anhui, Jiangsu, Shanghai and Zhejiang; SE China: Jiangxi, Fujian and Taiwan; Central China: Hunan and Hubei; South China: Guangxi and Hainan).

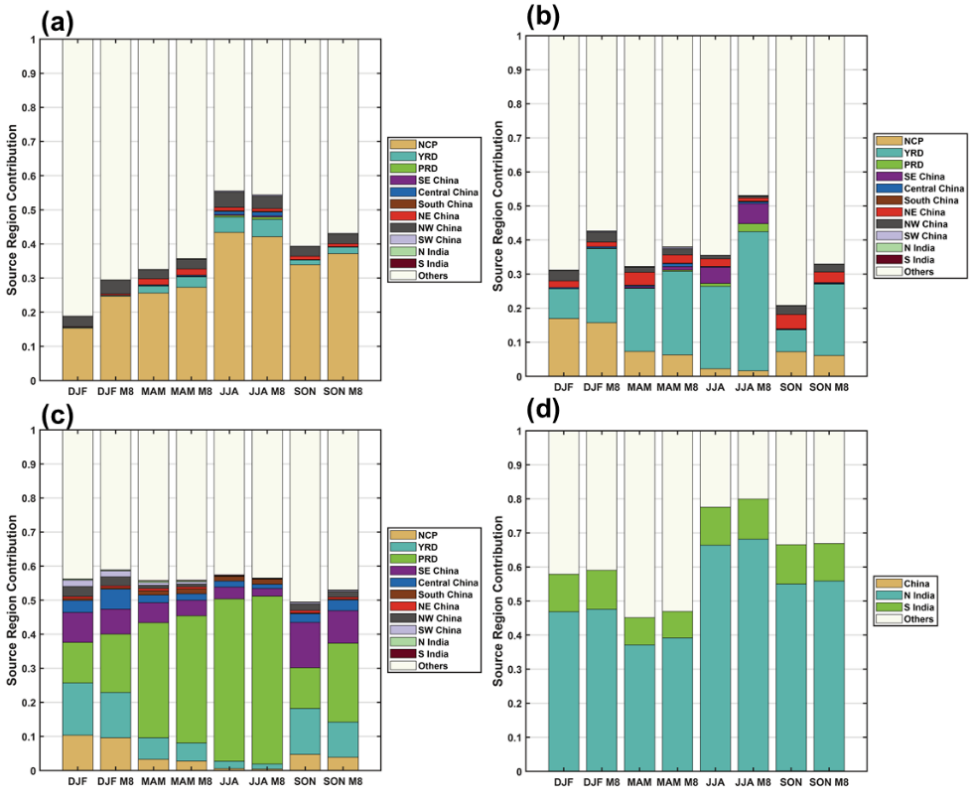

Fig. 8. Contributions to seasonally daily mean ozone (DJF, MAM, JJA, and SON) and MDA8 ozone (DJF M8, MAM M8, JJA M8, and SON M8) in Beijing (a), Shanghai (b), Guangzhou (c), and New Delhi (d) from different source regions.